Computers in Biology and Medicine 94 (2018) 74–84

Contents lists available at ScienceDirect

Computers in Biology and Medicine

journal homepage: www.elsevier.com/locate/compbiomed

Design of complex bone internal structure using topology optimization with perimeter control

Jaejong Park [a], Alok Sutradhar [a,*], Jami J. Shah [a], Glaucio H. Paulino [b]

[a] Department of Mechanical and Aerospace Engineering, The Ohio State University, Columbus, OH 43210, USA
[b] School of Civil and Environmental Engineering, Georgia Institute of Technology, Atlanta, GA 30332, USA

ARTICLE INFO

Keywords:
Bone
Internal structure
Topology optimization
Perimeter control

ABSTRACT

Large facial bone loss usually requires patient-specific bone implants to restore the structural integrity and functionality that also affects the appearance of each patient. Titanium alloys (e.g., Ti-6Al-4V) are typically used in the interfacial porous coatings between the implant and the surrounding bone to promote stability. There exists a property mismatch between the two that in general leads to complications such as stress-shielding. This biomechanical discrepancy is a hurdle in the design of bone replacements. To alleviate the mismatch, the internal structure of the bone replacements should match that of the bone. Topology optimization has proven to be a good technique for designing bone replacements. However, the complex internal structure of the bone is difficult to mimic using conventional topology optimization methods without additional restrictions. In this work, the complex bone internal structure is recovered using a perimeter control based topology optimization approach. By restricting the solution space by means of the perimeter, the intricate design complexity of bones can be achieved. Three different bone regions with well-known physiological loadings are selected to illustrate the method. Additionally, we found that the target perimeter value and the pattern of the initial distribution play a vital role in obtaining the natural curvatures in the bone internal structures as well as avoiding excessive island patterns.

1. Introduction

The internal architecture of bone is complex and remodels continuously. The stress trajectories and material distribution in human bone have been studied extensively. Also, a lot of efforts have been invested in understanding the evolution of the internal architecture of bone and their physiological loading [1,2]. Under the assumption that it achieves maximum mechanical stiffness with minimum mass, bone is considered to be structurally optimized where it adapts to long-term loading by controlling its density and internal structure [3–5]. Lanyon and Rubin [6] further reported that bone showed apposition only when *dynamically* loaded. Living bone continuously remodels itself by growth, reinforcement, and resorption. This complex multiphysics phenomenon has been broadly studied since the pioneering works in the 1960s. Among the earlier works, Cowin and Hegedus [7] proposed the use of a thermo-mechanical model that considers chemical reaction with a mass transfer within two constituents to model the bone remodeling. The model described therein predicts strain stimulated remodeling process that takes place in porous elastic solids. Authors found the bone remodeling prediction qualitatively agrees with the clinical observation of bone remodeling features. Carter et al. [8] suggested proportional relations between bone strength, modulus and the strain rate which can be used to predict bone tissue strength and stiffness through compression test of human and bovine trabecular bone specimens. Their work led to a mathematical (self-optimizing) theory that relates bone density, orientation, and stress [9]. Huiskes et al. [10] assumed Strain Energy Density (SED) as the stimulus for bone growth and proposed adaptive bone remodeling theory for prosthetic design. Beaupre et al. [11,12] handled both the internal and external remodeling simultaneously as time-dependent surface-mediated phenomena followed by energy effective stress stimulus from load history. Weinans et al. [3] combined this time-dependent remodeling rule with per element (apparent SED based) stimulus in Finite Element Analysis (FEA) to investigate the stability and convergence behavior in proximal femur which disclosed good morphological similarity to reality. Many of the aforementioned works model the bone remodeling as a combination of the mechanical and biological process with various assumptions on mechanical stimulus.

Recent advances in high-performance computing and additive manufacturing have also made it possible to create patient-specific biomedical implants replacing bones. Typically, porous coatings are

* Corresponding author.
E-mail address: sutradhar.1@osu.edu (A. Sutradhar).

https://doi.org/10.1016/j.compbiomed.2018.01.001
Received 15 September 2017; Received in revised form 5 January 2018; Accepted 6 January 2018

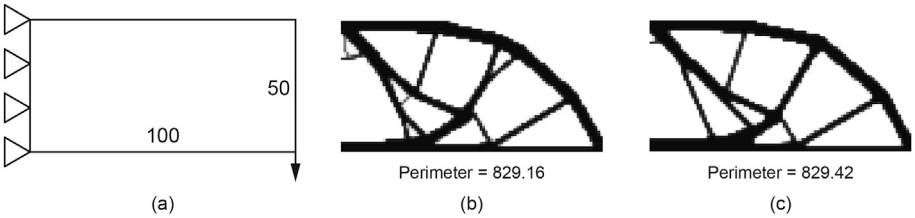

Fig. 1. Cantilever problem, (a) design domain (2:1 aspect ratio discretized by 100×50 Q4 elements) and boundary condition, (b) result from regular compliance minimization without perimeter constraint, (c) active perimeter constraint ($P_{min} = 830$).

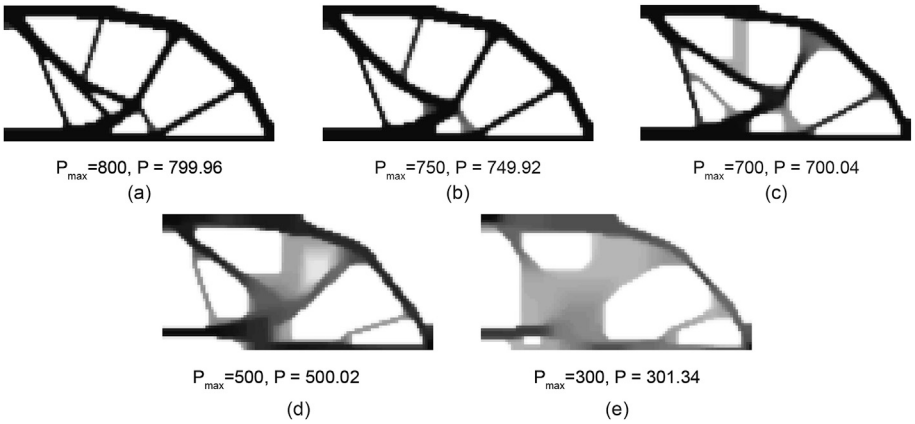

Fig. 2. Maximum perimeter value, P_{max}, is progressively reduced in the Cantilever problem. (a) $P_{max} = 800$, (b) 750, (c) 700, (d) 500, (e) 300. Following number, P in the figure, represents the achieved perimeter.

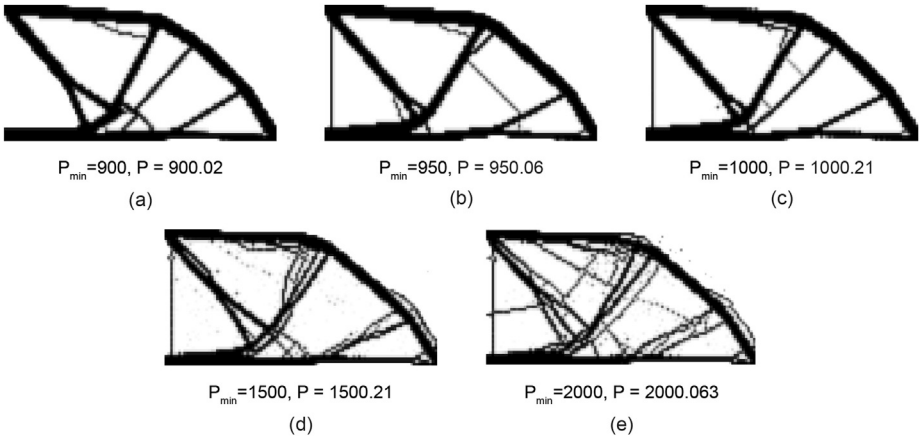

Fig. 3. Minimum perimeter value progressively increased in the Cantilever problem. (a) Minimum perimeter 900, (b) 950, (c) 1000, (d) 1500, (e) 2000. Following number, P in the figure, represents the achieved perimeter.

used at the interface of these implants and the surrounding bone to increase the stability of the implants and the bone tissue in-growth. Titanium alloys (e.g., Ti-6Al-4V) have been used to fulfill the requirements of low stiffness, high strength, and good corrosion and fatigue resistance [13]. Nevertheless, these implants exhibit a mechanical property mismatch with surrounding bone tissue leading to stress-shielding [14]. This results in unfavorable stress, irregular bone healing, and undesired bone remodeling. The biomechanical mismatch can also vary within patients, locations, and dimensions [15,16]. To address the stiffness imbalance in the case of the traditional solid cage, various pillar structures were designed and tested in intervertebral cages [17]. Also, the improvement of the regular Ti-6Al-4V bone scaffolds was proposed employing analytic solutions for particular beam networks that consist of the scaffold geometries [18]. To create the next generation of implants, understanding and mimicking the bone internal structure through a design methodology is of immense importance for the design of the implant and the subsequent remodeling. In this regard, current work attempts to bridge a numerical optimization technique with the *design of implants* which has trabeculae-like internal structure.

Topology optimization formulated for compliance minimization can be a good candidate in serving as the essential tool to study bone internal architecture. Topology optimization provides the optimized material layout within a given computational design domain for prescribed boundary conditions so that the resulting material arrangement satisfies a set of required performance goals. The basic concept of the popular density based method is to represent the geometry as a rasterized image where the color of each pixel corresponds to the value of a physical parameter [19]. The method iteratively updates the material field based on the performance of the current design and sensitivity information of each parameter. Unlike traditional structural optimization methods, topology optimized structures can be massively different compared to the initial geometry and do not require any geometric feature *a priori*. This makes topology optimization suitable for early design stages by giving insightful ideas to the designer and providing a wide variety of design options for distinct problems across different scales [19–22]. Topology optimization has proven as a powerful design tool in aerospace engineering [23], and other industrial design applications [24–26], among others.

Topology optimization has been used to predict bone density distribution and to obtain rough estimates of the bone internal structure. Rossi

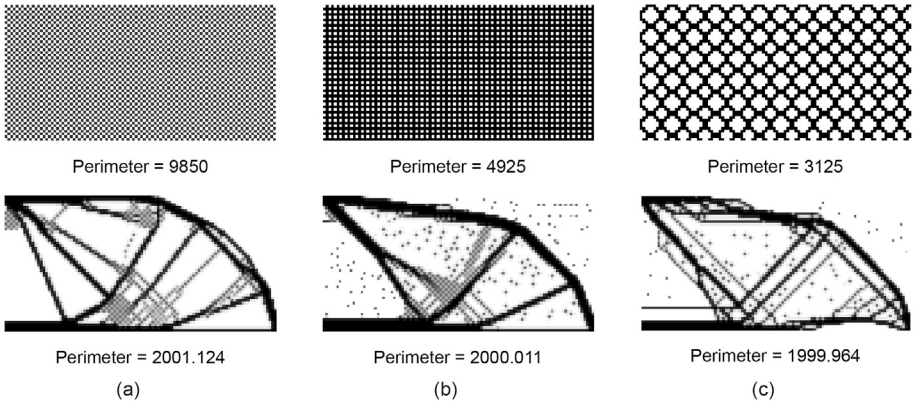

Fig. 4. Cantilever problem is optimized with a perimeter constraint value of 2000. Regular patterns in initial density distribution are used. (a). Checkerboard, (b). Regular square pattern, (c). Regular circular pattern. Numbers represent the perimeter. Checkerboard patterns and density islanding are visible in the results.

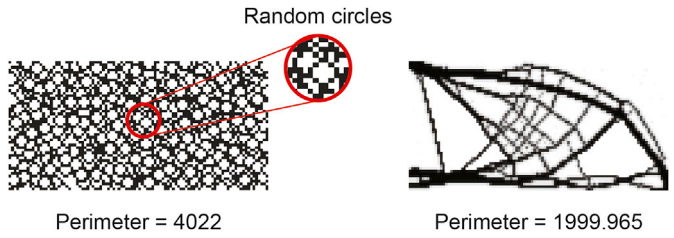

Fig. 5. Random circles (left) are used in the initial density distribution for the cantilever beam problem. With perimeter target of 2000, the topology on the right is obtained. Pattern preservation or density islanding is significantly reduced in the result.

and Wendling-Mansuy [27] used a laminated anisotropic microstructure to propose a bone adaptation model. Xinghua et al. [28] used topology optimization to simulate the external shape and internal density distribution of human femur and vertebrae. In the field of bone remodeling, the trabecular adaptation was studied in Refs. [29–31] using a design space optimization. An iterative remodeling scheme has been proposed in Ref. [32] with a remodeling rate equation that maximizes the structural stiffness (minimizing the total bone strain energy) in each time step for a time-dependent loading in the human proximal femur.

Fibrous trabecular architecture can be obtained by introducing a restriction on the perimeter in the topology optimization formulation. Perimeter control originally emerged in topology optimization to mitigate the numerical instabilities by limiting the maximum perimeter [33]. A minimum value of the perimeter can be prescribed to attain structures with thin members resulting in increased perimeter value in the design suitable for capturing bone trabecular architecture. In general, additional design constraints directly affect the design update by slowing the convergence rate and possibly directing the solution to undesired local minima. In this work, we attempt to accelerate the convergence by employing various patterned structures as initial designs. The results from numerous biomedical examples indicate this approach achieves the necessary geometric complexity in a controlled manner. We believe that current work can bring positive impact on not only the performance of current bone implants but also design problems that involve geometrically complex structures.

The rest of the article is organized as follows: Section 2 discusses the general topology optimization, and the method used to treat perimeter control constraint. Section 3 shows the numerical implementation of the formulation along with interesting findings on initial density distribution. The section also showcases various biomedical examples including femur, calcaneus, and midface. Section 4 summarizes the study and its overall contributions.

2. Methods

In this section, the approach employed in this work to obtain natural looking bone internal structure designs is shown. First, the conventional topology optimization for compliance minimization under a volume fraction constraint is discussed. The problem is cast as a material distribution problem in topology optimization. The perimeter constraint that allows the user to control the sum of the length of inner and outer boundaries is also explained. By combining these two ideas, we seek to acquire the optimized structure with controlled topological complexity.

2.1. Topology optimization for minimum compliance

Topology optimization is a branch of structural optimization which originated from Ref. [34]. This method iteratively distributes materials available in a design domain to give an optimized structure for an objective function. A typical topology optimization algorithm combines two distinct modules; one for analysis and the other for optimization. In

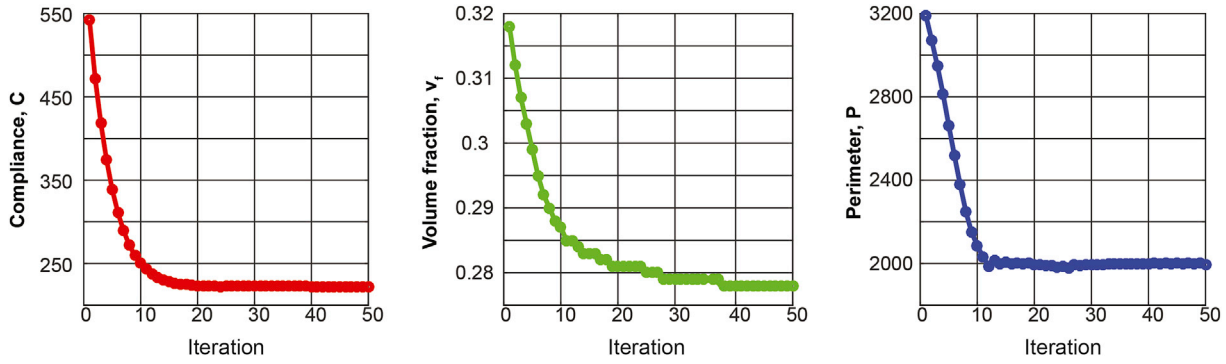

Fig. 6. Convergence plots of compliance, volume fraction, and perimeter value for cantilever beam problem with random circular patterns are shown.

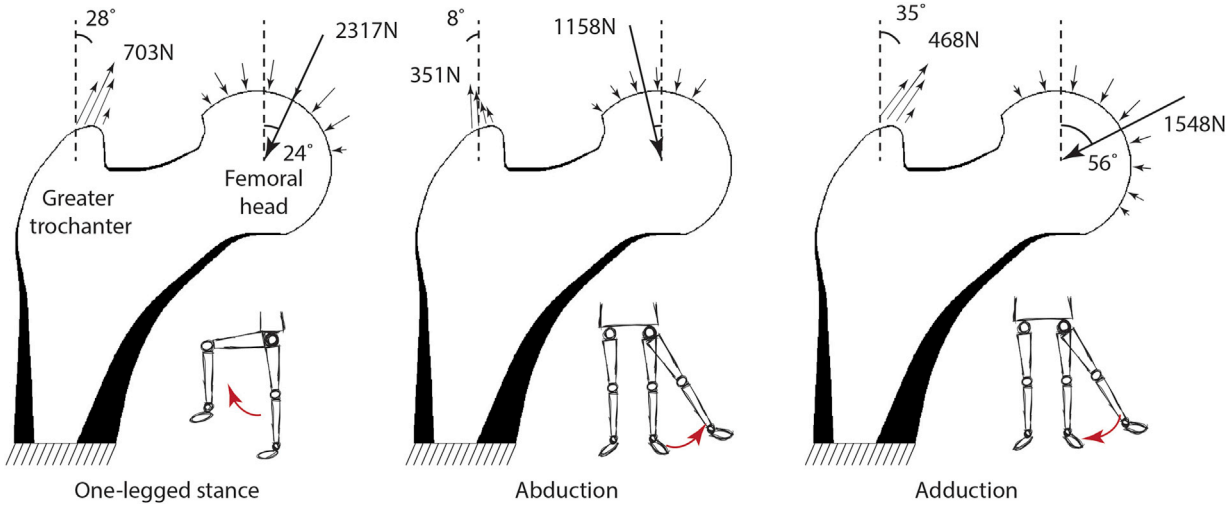

Fig. 7. Numerical representation of three common daily loadings on the proximal femur is shown.

each iteration, the design is updated based on the structural performance obtained from the finite element analysis. A common topology optimization formulation is the compliance minimization. In this setting, the resulting structure evolves to have the maximum possible stiffness under certain constraints (e.g., a volume fraction constraint) for given loads and boundary conditions. Consider a design domain $\Omega \in R^2$ or R^3. The discrete topology optimization problem statement reads as,

$$\begin{aligned} &\min_{\rho} \Phi(\boldsymbol{\rho}, \mathbf{u}(\boldsymbol{\rho})) \\ &s.t. \quad : \int_{\Omega} v\rho \mathrm{d}\Omega = \sum_{e=1}^{N} v_e \rho_e \leq V^* \\ &\qquad \mathbf{K}(\boldsymbol{\rho})\mathbf{u} = \boldsymbol{f}, \\ &\qquad g_i(\boldsymbol{\rho}, \mathbf{u}(\boldsymbol{\rho})) \leq g_i^*, \quad i = 1, \ldots, M \\ &\qquad \rho_e = \begin{cases} 0 & \text{void}, \\ 1 & \text{material}, \end{cases} \quad e = 1, \ldots, N \end{aligned} \tag{1}$$

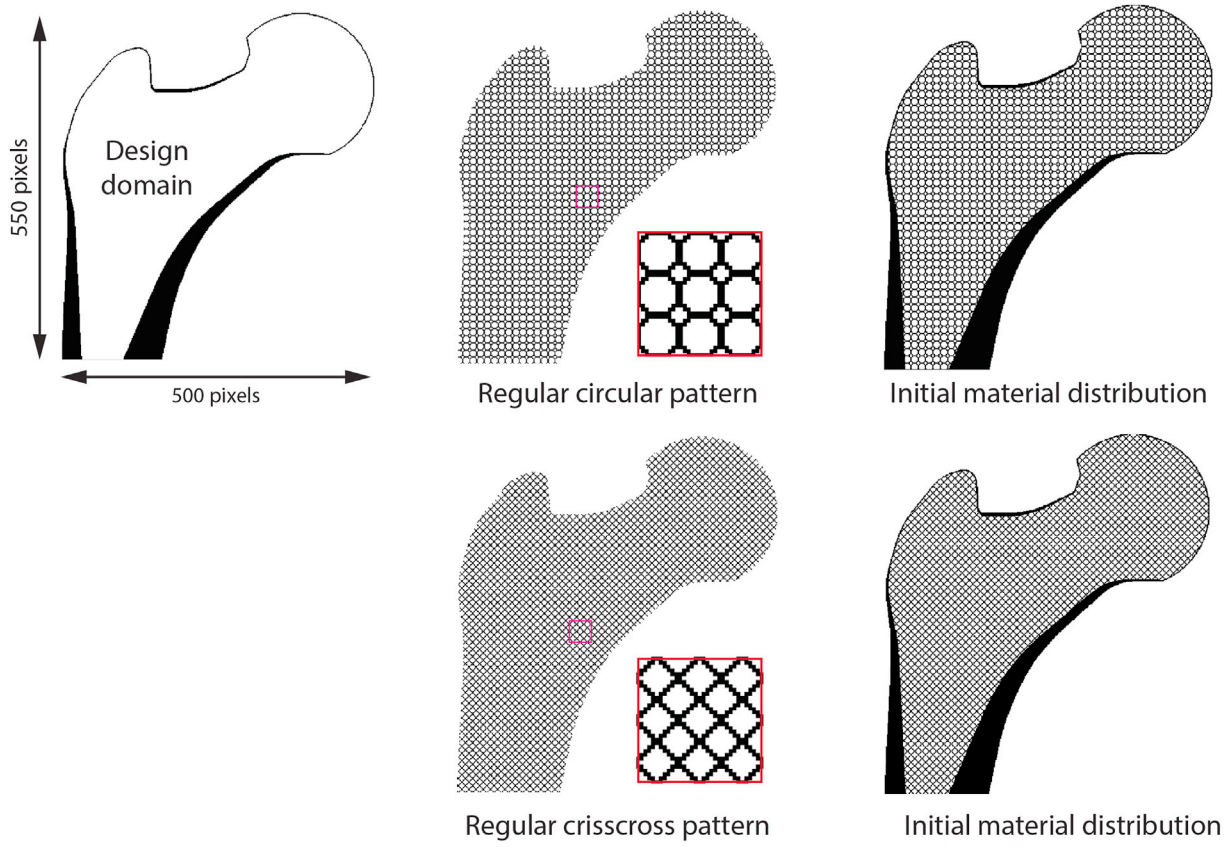

Fig. 8. Design domain for proximal femur model and regular patterns (circular and criss-cross) in the initial density distribution.

where Φ is the compliance, $\boldsymbol{\rho}$ is the density vector, $\mathbf{u}$ is the global displacement vector, v_e is the elemental volume, ρ_e is the elemental density, V^* is the prescribed volume fraction and N is the number of elements. The first constraint describes the maximum allowable volume in the result. The second constraint is the equilibrium equation where $\mathbf{K}$ is the global stiffness matrix, $\boldsymbol{f}$ is the global load vector. The third constraint (g) is a set of M different functions which describe generic design or performance requirements that depend on the design variable $\boldsymbol{\rho}$ and the state variable $\mathbf{u}$. However, this integer optimization problem is considered mathematically intractable. Allowing the density to vary makes the objective function and the constraints both continuous and differentiable.

$$0 \leq \rho \leq 1, \tag{2}$$

There have been several approaches that account for the material model with intermediate densities. An approach named Solid Isotropic Material with Penalization (SIMP) was proposed [35] and later improved in Ref. [36]. In modified SIMP, the elastic property of elements is obtained as,

$$E(\rho) = E_{min} + \rho^p\left(E^0 - E_{min}\right). \tag{3}$$

Here, E_{min} is a small stiffness applied to void regions in order to avoid singular stiffness matrix, p is the penalization factor generally chosen as 3 to steer intermediate densities to either extreme (0 or 1), and E_0 is the elastic property of the base material. Additionally, the gradient of the compliance, $\frac{\partial\Phi}{\partial\rho_e}$, needs to be computed, and each element density value is updated based on this sensitivity information. $\frac{\partial\Phi}{\partial\rho_e}$ has the closed form expression as follows,

$$\frac{\partial\Phi}{\partial\rho_e} = -p\rho_e^{p-1}\left(E^0 - E_{min}\right)\mathbf{u}_e^T\mathbf{K}_0\mathbf{u}_e, \tag{4}$$

where $\mathbf{K}_0$ is the constitutive matrix with unit Young's modulus and $\mathbf{u}_e$ is the displacement vector of an element e.

There have been numerous techniques developed for solving topology optimization including Optimality Criteria (OC), Sequential Linear Programming (SLP), Sequential Quadratic Programming (SQP), Convex Linearization (CONLIN), etc. OC updates the design variables (ρ in the current formulation) proportionally to the objective function values. It is known to be simple and efficient for optimization problems with a single constraint [19]. SLP locally linearizes a nonlinear problem at a design point then optimizes within move limits that bound the admissible region. CONLIN uses variables that characterize the optimization problem to perform linearization of the original problem. Method of Moving Asymptotes (MMA) [37] falls into this category because it uses aggressive moving asymptotes as function characterizing parameters to ensure stability and convergence speed. In this work, we have used MMA to handle the additional perimeter constraint. Readers are referred to [38,39] for more in-depth discussions and explanations on different optimization techniques used in topology optimization.

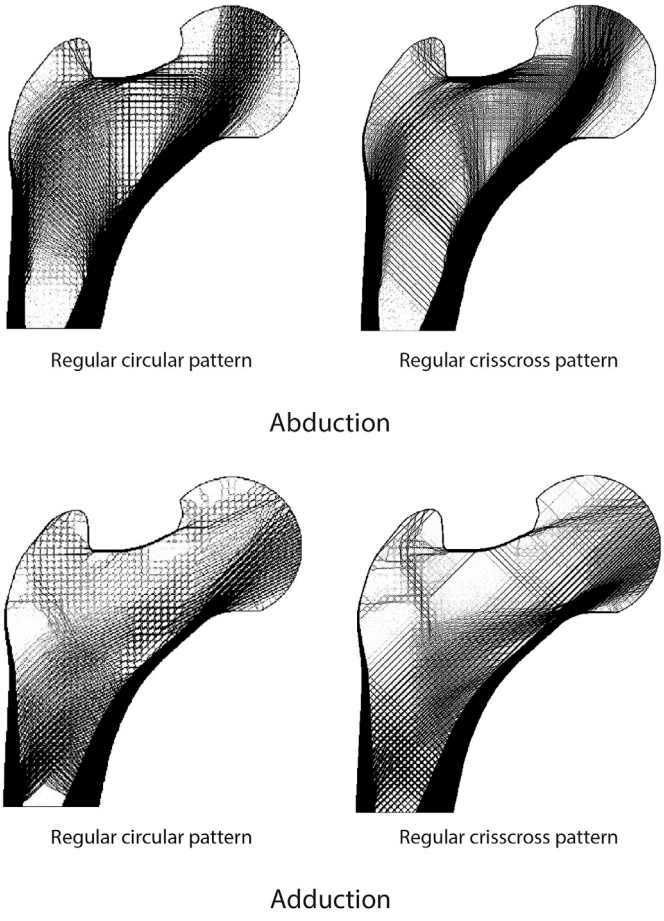

Fig. 9. Femur results for abduction and adduction with regular patterns. The initial patterns are retained (i.e., bias exists) in the final result.

2.2. Perimeter control constraint

Perimeter control constraint was introduced in conventional topology optimization to alleviate these checkerboard effects [33]. The checkerboard pattern is a numerical instability seen in results of the topology optimization and refers to areas containing alternating solid and void elements [40,41]. A perimeter of a structure is defined as the length of inner and outer boundaries. In the current problem setting, the perimeter would be the total variation of density distribution in design domain, perimeter ($P(\rho)$) of a 2-dimensional structure with void elements ($\rho = 0$) surrounding it can be mathematically calculated similarly to [33] as follows,

$$P(\rho) = \int_{\Omega} |\nabla\boldsymbol{\rho}| \mathrm{d}\Omega. \tag{5}$$

By constraining the maximum perimeter, larger void regions can be obtained. Inversely, the larger void regions can be divided into smaller voids with a constraint on the minimum perimeter. The following can be added to the original topology optimization problem in Equation (1) to specify a lower bound on the perimeter,

$$P \geq P_{min}, \tag{6}$$

where P_{min} is the minimum perimeter value allowed in the final solution.

The sensitivity of the perimeter constraint is necessary for the update of the density values. The perimeter sensitivity is formulated similar to [30] for the case of square elements in 2D rectangular domain as,

$$\frac{\partial P(\rho)}{\partial\rho_e} = \sum_{j=0}^{A}\sum_{i=1}^{B}\mathscr{L}\cdot\frac{\partial\rho_{i,j}}{\partial\rho_e}\cdot sign\left(\rho_{i,j} - \rho_{i-1,j}\right) + \sum_{i=0}^{B}\sum_{j=1}^{A}\mathscr{L}\cdot\frac{\partial\rho_{i,j}}{\partial\rho_e}\cdot sign\left(\rho_{i,j} - \rho_{i,j-1}\right), \tag{7}$$

where $\mathscr{L}$ is the edge length of an element $A \times B$ represents the mesh size of the design domain and $sign(x)$ is the sign function of the real variable x.

Note that the minimum perimeter constraint can potentially lead to checkerboard patterns in the final solution. A linear filter is employed to the density fields to reduce this effect as follows,

$$\tilde{\rho}_e = \frac{\sum_{\Omega_e} w_{ne}\cdot\rho_e}{\sum_{\Omega_e} w_{ne}}, \tag{8}$$

where $\tilde{\rho}_e$ is the filtered density value, and $w_{ne} = max(0, r_{min} - dist(n, e))$ is

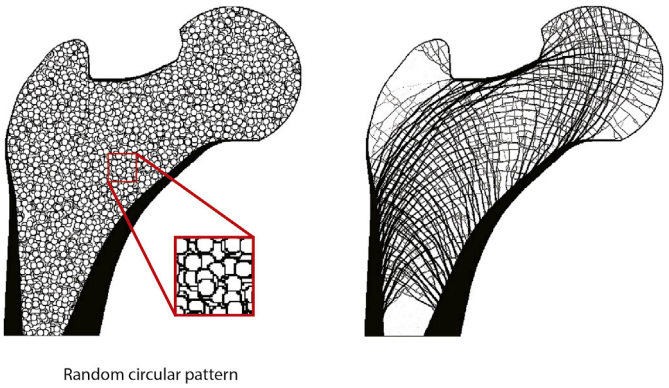

Fig. 10. Femur result for combined loading (with a ratio of 3:1:1 for one-legged stance, abduction, and adduction) with random circular patterns.

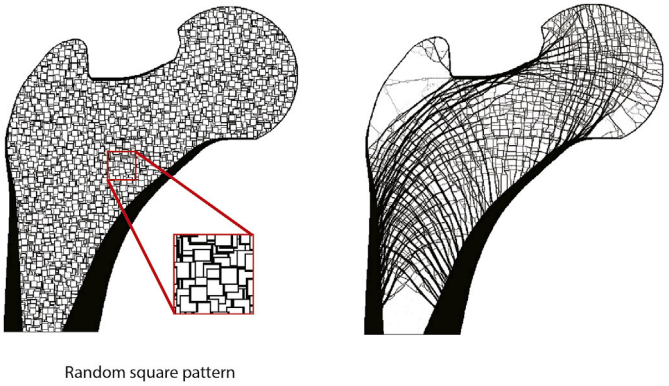

Fig. 11. Femur result for combined loading (with a ratio of 3:1:1 for one-legged stance, abduction, and adduction) with random square patterns.

defined as the distance function between the center of the filter (n) to elements (e) within the zone of filter influence Ω_e with a radius of r_{min}.

3. Numerical implementation

In this section, we demonstrate the implementation using the cantilever beam which is a popular benchmark problem in topology optimization. We first ran the problem without the perimeter control and calculated the perimeter value of the reference result. Targeting the reference perimeter, another result with perimeter control was obtained and compared with the reference result. We then show the necessity of modifications in the initial material distribution to avoid numerical artifacts.

3.1. Cantilever beam with uniform initial density distribution

A design domain with an aspect ratio of 2 (length) to 1 (height) is fixed on the left edge. This design domain is subjected to a vertical point load in the bottom-right corner as shown in Fig. 1(a). The domain is discretized with 100×50 Q4 elements. Design parameters include a volume fraction constraint of 30%, penalization factor of 3, and linear filter with a size of 1.2 of a Q4 element. The SIMP approach without any constraint on the perimeter yields the result shown in Fig. 1(b). This reference gives a perimeter of 829.16 according to Equation (5). We add a constraint which defines the limit of 830 on the perimeter to the same problem to compare the result with the reference in Fig. 1(b). The perimeter-constrained solution is provided in Fig. 1(c). Both of the results are obtained from the same uniform initial distribution.

Results in Fig. 1(b) and (c) look similar since most of the major members are located in the same place. However, they are not identical since the result in Fig. 1(c) was obtained considering the perimeter sensitivity in Equation (7) during the design update, whereas the result in Fig. 1(b) was not.

We first look at the effect of decreasing the target perimeter value. To achieve this, $P \leq P_{max}$ replaces the constraint in Equation (6). The maximum perimeter, P_{max}, is prescribed while all other parameters are kept the same. Starting from the reference perimeter 830, perimeter constraint values are decreased gradually until 40% (i.e., 800, 750, 700, 500, and 300). Uniform initial density distribution is used for all results. The results are provided in Fig. 2.

Topology optimization with perimeter constraint gives a result with no numerical issues if the target perimeter value is close to the reference as in 800, 750, 700 cases in Fig. 2. The desired perimeter value is achieved by removing the least necessary set of members from results in Fig. 1(b) and (c). However, gray regions start to form as the target perimeter is set far from the reference value. These gray regions are not coveted in topology optimization since they are regions with intermediate density values which is not realistic.

The values are progressively increased up to 400% from the reference value of 800 (i.e., 900, 950, 1000, 1500, and 3000). Perimeter constraint now defines a lower limit on the perimeter, and thereby the perimeter is increased in the same design domain. Again, all other design parameters are kept the same. Fig. 3 presents the result from the increasing target perimeter.

A higher perimeter value is obtained either by creating more members or by branching if the constraint value is close to the reference value in Fig. 1(b). Density islands are formed when the target perimeter is significantly greater than the reference value. Density islands are not desirable because it does not improve the performance of the structure. The current algorithm leads the solution to converge to unacceptable local minima when target perimeter is set far from the reference value. Thus, we attempt to alleviate the issue by modifying the initial density distribution in the next subsection.

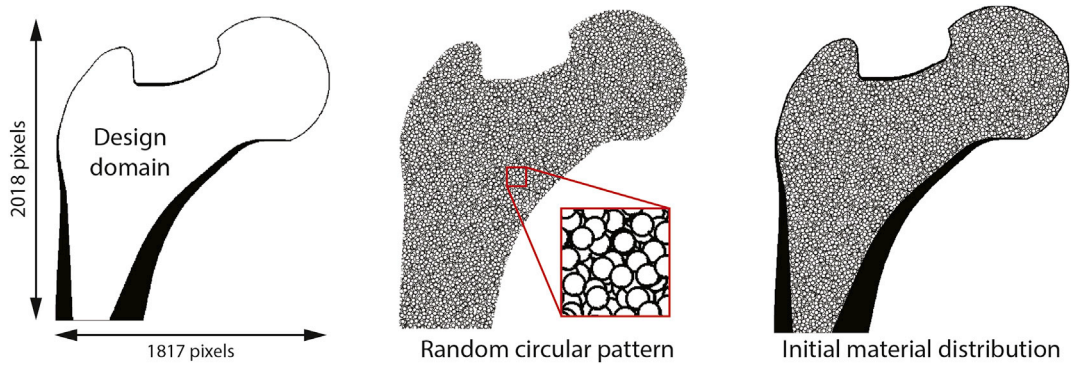

Fig. 12. Design domain with higher resolution (2018×1817 Q4 elements) for proximal femur model and random circular patterns in the initial density distribution.

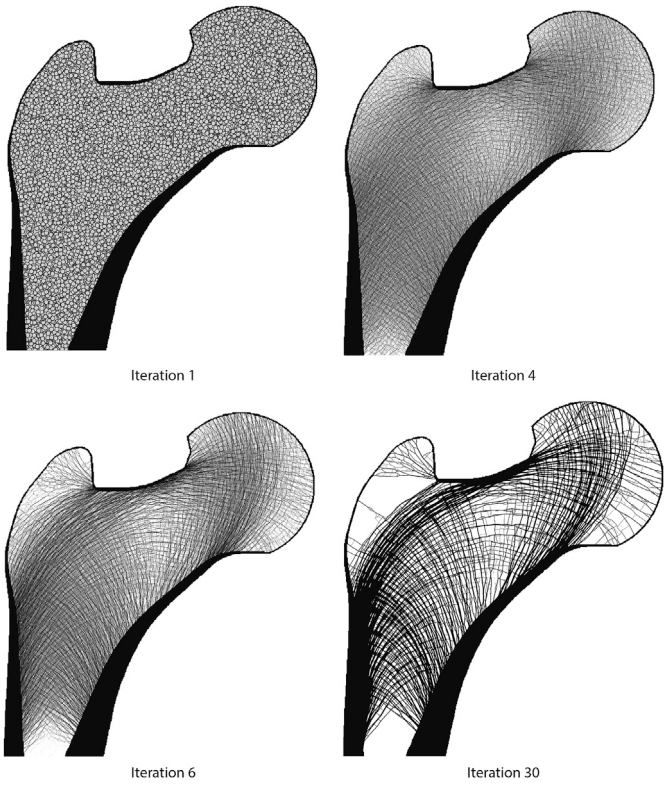

Fig. 13. Design evolution is shown using intermediate results.

3.2. Effects of the initial density distribution

The state problem that is solved in topology optimization can be complex with many potential extreme points and thus, depends heavily on the initial density distribution. Due to this fact, various initial density distributions are tested for the cantilever problem to check whether the preferred convergence can be achieved. The rectangular design domain with the same discretization and cantilever boundary condition with a target perimeter (P_{min}) value of 2000 is considered for all numerical examples in this subsection. Other parameters such as filter size and penalization factor remain as 1.2 and 3, respectively. First, simple regular patterns including checkerboard, rectangular, and circular grids are used as initial density distribution. The results with these regular patterns in the initial design are presented in Fig. 4.

The results indicate that topology optimization gives results without numerical artifacts if the initial perimeter value is close to the target value. A large discrepancy between the initial and target perimeter leads to stability issues in the form of islanding and checkerboard patterns. Another important observation is that the initial density distributions with regular patterns retain the same pattern in the final result. Although this phenomenon can be useful in some pattern design applications, it creates bias in the solution during the update from its initial density distribution. Consequently, *randomness* can be introduced in the initial density distribution to remedy the bias. The design domain with 700 overlapping circles with a radius of 5 (*pixels* or elements) is used to test this hypothesis. Each circle is placed at randomly selected points. With all the other parameters kept as is, the result in Fig. 5 is obtained. The convergence plots for compliance, volume fraction, and perimeter are provided in Fig. 6.

The introduction of randomness reduces the undesired numerical artifacts in the design. Design bias is not noticeable, and the islanding phenomenon is substantially mitigated even with a significant difference in the original perimeter (4022) and the target (2000). However, density islanding has not completely removed. This is because the objective and the perimeter control constraint are conflicting. In the present setting without any modification, careful selection of initial design pattern and design parameters such as volume fraction and target perimeter is necessary in some cases. One can enlarge the filter to limit the minimum feature size yet this may affect the desired geometric complexity in the solution. Another procedure would be to filter out the isolated islands during the iterations which may add an extra functional relation between the design variable and physical density values. Undesired numerical artifacts can be minimized if the perimeter and the volume fraction between the initial density distribution and the target values are close to each other.

4. Bone internal structure

The proposed approach is applied to mimic the internal structures of three bone regions: the human femur, ovine calcaneus, and human midface. The human proximal femur has been widely used in various computational studies due to common total hip replacement and implant placement. The femur is attached to the pelvis and is responsible for not only supporting weights from the torso but also forces associated with the daily activities including one-legged stance, adduction, and abduction (See Fig. 7). Its trabecular architecture is believed to be efficiently formed for these loading conditions. We also use the methodology in designing the internal structure of calcaneus of ovine using simple cantilever beam-like boundary conditions.

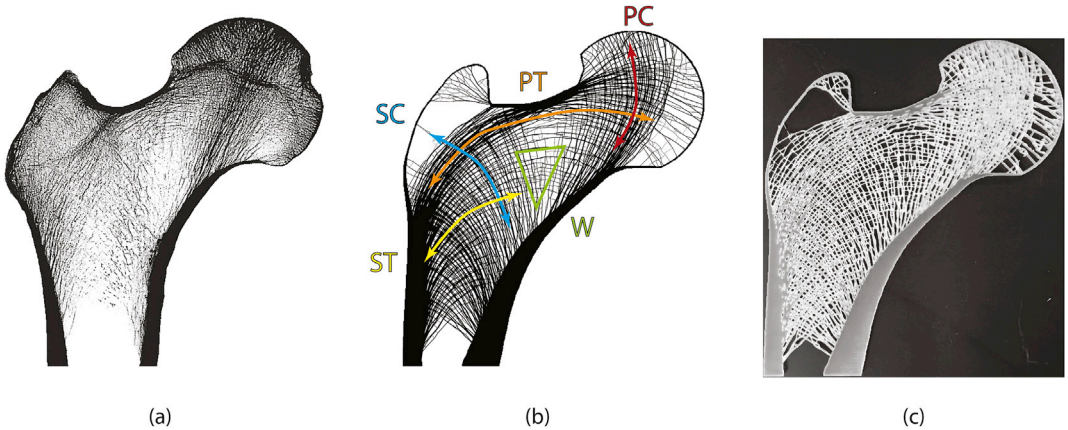

Fig. 14. Comparison between (a) X-ray of the femoral head and (b) femur model from topology optimization with perimeter constraint on 2018 × 1817 discretization. All key load transfer paths can be observed in the result. (c) Topology optimized femur model from 550 × 500 grid is 3D printed using material jetting (3D systems Projet 3500 HDmax with VisiJet M3 Crystal).

4.1. Human proximal femur

The cross section of the femur from the frontal plane is selected as the model for the study. The joint reaction force of 2317*N* directed 24° from the vertical axis, and hip adductor force of 703*N* at 28° from the vertical axis are distributed using a quadratic distribution function on the femoral head and the greater trochanter, respectively to represent the one-legged stance as shown in Fig. 7. Abduction and adduction are modeled similarly to [30,42,43]. These works also report that typical human daily activity gives 3:1:1 frequency ratio for the one-legged stance, abduction, and adduction, respectively. These multiple loading conditions and the corresponding frequency factors are all considered in the topology optimization problem.

4.1.1. Regular pattern

The femur cross-section is discretized into a 500×550 grid. The active design domain (trabecular region) confined by the non-designable cortical bone region is filled with regular patterns: regular circles (5-pixel radius) and crisscross. The regular pattern with circles gives the perimeter of 56,480 whereas crisscross produces a value of 72,830. A schematic of the initial material distributions is provided in Fig. 8.

The target perimeter is chosen to be 70,000, which is close to the initial perimeter to minimize the density islanding, for the two separate loading conditions (abduction and adduction) for both initial material distributions. A linear filter with a radius of 1.2 is used, and the volume fraction is constrained at 0.3.

As shown in Fig. 9, initial patterns are retained in the results for both loading conditions for the regular circular and criss-cross patterns. This bias is undesirable because it limits the design options such as curved members.

4.1.2. Random pattern

Random patterns can be used for the initial material distribution to mitigate the bias issue and alleviate factors that may restrict the designs. Two different random patterns are tested for this hypothesis. The same design domain is now filled with 1) circles with 5-pixel radius and 2) squares with 6-pixel sides, both located randomly with each overlapping each other. One-legged stance, abduction, and adduction are all considered in this analysis with weights of 3, 1, and 1, respectively. Perimeter values (P) are calculated to be 68,816 and 79,846 for random circles and random squares, respectively. The target perimeter value is selected to be 60,000 for both cases with volume fraction constraint of 0.3. The linear filter covers the circular region with a radius of 1.2 elements. Two random initial material distributions and their respective results are provided in Figs. 10 and 11.

Important to note, utilizing random patterns in the initial material distribution leads to very similar internal architectures. The initial pattern bias is minimal in both the solutions. Also, members have various curvatures to create more natural-looking structure.

The computational domain is further discretized in an attempt to further eliminate the pattern bias and generate a more refined result with a room for more geometric features in the design. The new domain is discretized into 2018×1817 by roughly doubling the pixel densities in both directions. Twenty thousand circles with a radius of 14 are randomly placed using the same algorithm leading to an initial perimeter of 426,535 as shown in Fig. 12. The volume fraction constraint remains equal to 0.3, and the target perimeter is chosen as 300,000.

The evolution of the solution is shown in Fig. 13 with intermediate designs displayed at selected iterations. The final result is compared with the functional groups in the X-ray of the human femur in Fig. 14. A topology optimized femur model is also 3D printed using the jetting machine (3D systems Projet 3500 HDmax with VisiJet M3 Crystal) with 16 μm layer height and shown in Fig. 14(c).

4.2. Ovine calcaneus

Calcaneus (heel bone) experiences significant compressive loading while walking which can be modeled as a simple cantilever-beam like loading scenario. Topology optimization was also previously used to investigate the internal bone architecture of ovine calcaneus in Ref. [44]. They found that typical minimization of strain energy under the aforementioned boundary condition results in simplistic structure when compared to the X-ray of an ovine calcaneus although the direction of core members are in the same direction. The same problem is solved with the perimeter control constraint presented in this work. The same design domain and the boundary conditions are extracted from earlier work in Ref. [44] and discretized by 352×709 Q4 elements. The active design domain is filled with 7000 circles with a radius of 5 at randomly selected locations, resulting in an initial perimeter of 87,850. The design problem and the initial random material distribution are shown in Fig. 15.

With a target perimeter of 60,000 and using 0.3 for volume fraction constraint, the following solution in Fig. 17 is obtained. The evolution of the result is provided in Fig. 16.

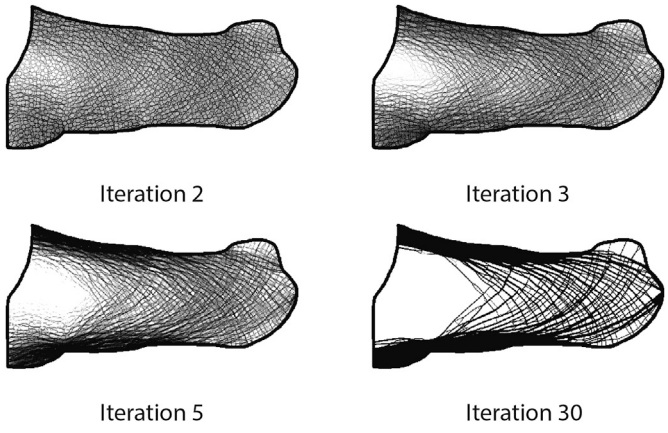

Fig. 16. Evolution of solution for the ovine calcaneus problem is provided.

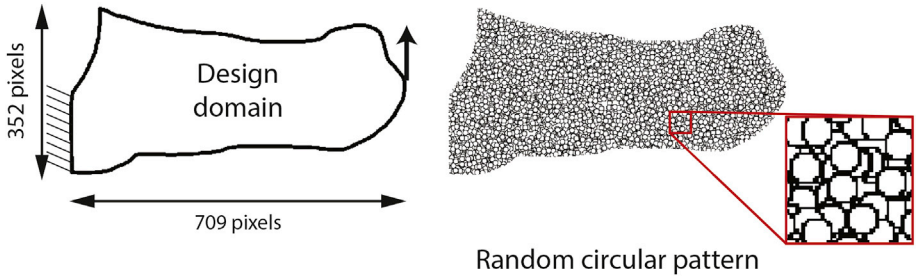

Fig. 15. Design domain and boundary condition for calcaneus model and random circular patterns in the initial density distribution.

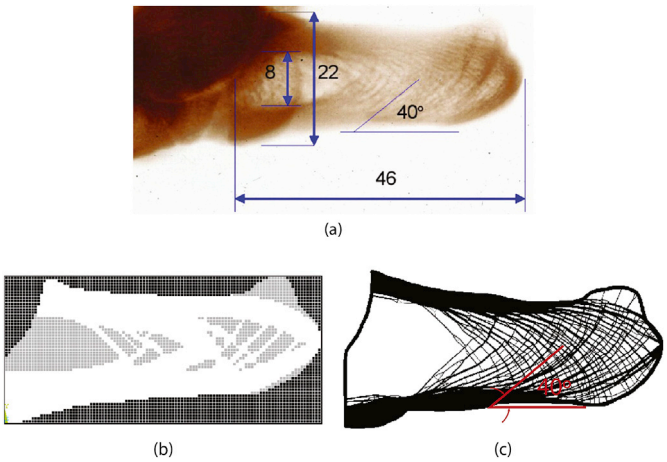

Fig. 17. Comparison between (a) X-ray of the ovine calcaneus, (b) Result from Kim et al. [44] by topology optimization without design restrictions, and (c) Result from topology optimization with perimeter control $P_{min} = 60,000$.

The result from perimeter controlled topology optimization shows a good agreement with the X-ray scan of the ovine calcaneus.

4.3. *Internal structure in bone implant for midface reconstruction*

Human midface serves as crucial load transfer paths for forces from daily basic life functions such as breathing, speaking, chewing, and swallowing. It also forms the basis for the unique physical appearance of every human being. Sutradhar et al. [45,46] suggested using topology optimization to design implants in case of large facial injuries. Later, they proved that the topology-optimized shape sustains the maximum chewing load of 530*N* and also provides proper load transfer mechanism [47, 48]. It is also shown that cross-sectional geometry of human midface (on the vertical plane) through the first molar can be mimicked using 2D topology optimization with realistic supports, cavities, and loads (e.g., chewing and traumatic forces).

In this work, perimeter control constraint is added to design the internal structure of a bone implant to improve the structural efficiency and performance potentially. The design domain and the boundary conditions are adopted from Ref. [45]. The active design domain is patterned with 10,000 circles in randomly selected locations that have radius and thickness equal to 5 and 1 pixel, respectively, in a 608×402 discretization. This design domain and the boundary conditions are provided in Fig. 18(a) and (b). The initial perimeter is 46187, and the target optimization parameters are set as 30,000 for the perimeter and 20% for the volume fraction constraint. The filter size remains as 1.2 elements, and the penalization factor is set at 3. The result from topology optimization is shown in Fig. 18(c).

5. Discussion

Although the mechanical stimulus that was assumed may be different, the fundamental idea of bone remodeling researches have similarities [4]. They assume the bone is a nonlinear system and their behavior is represented by a family of differential equations. Also, these equations can be recast as element-wise optimization problems when combined with FEA. This allowed an application of structural optimization techniques to predict bone remodeling process. Garcia et al. [49] combined CAO, a shape optimization based on biological growth, with damage theory and in their later work, they applied it to predict remodeling behavior on the proximal femur after total hip replacement and implant placement [50]. They found that it can generate thermodynamically consistent solutions while predicting the vital physical effects including anisotropic remodeling criterion. In fact, the connection between the bone remodeling rate equation and the structural optimization of total strain energy was found in the 1990s [51]. Among many structural optimization techniques topology optimization gathered attention in modeling the bone remodeling process due to its similarity to earlier FE based bone remodeling models in that the density being the design variable; apparent density and normalized density. The microtrabecular bone architecture was realized using homogenization by calculating effective stiffness and stress [52]. Similarly, Jacobs et al. [53] found a full anisotropic elasticity tensor which was optimized for a given strain at each location in the bone. Along with anisotropic material parameters and time-dependent loading, a structural stiffness is iteratively maximized (compliance minimization) and it showed bone adaptation from altered loading [32]. Hybrid cellular automata (HCA) method incorporating the tissue level bone adaptation has been used in topology optimization to describe bone remodeling process [54]. It has been reported the structural optimization techniques tend to produce cancellous structures similar to bone [55]. Another interesting finding by Jang et al. [4] states that SED based bone remodeling algorithm and topology optimization for compliance minimization have mathematical analogies.

The present work shows how to obtain a trabeculae-like structure using topology optimization. The objective is to design a structure (e.g., a bone implant) that would efficiently withstand applied forces with different loading scenarios by minimizing deformation energy under a perimeter control constraint. Here, we found that the randomness in the initial design domain along with the perimeter control plays a crucial role in getting natural looking structural members with various curvatures. The purpose is to provide a tool that can produce a bone-like internal structure that is dominated by mechanical loadings rather than trying to understand the bone remodeling itself. Thus, we would want to emphasize that the algorithm described here to be more applicable to any

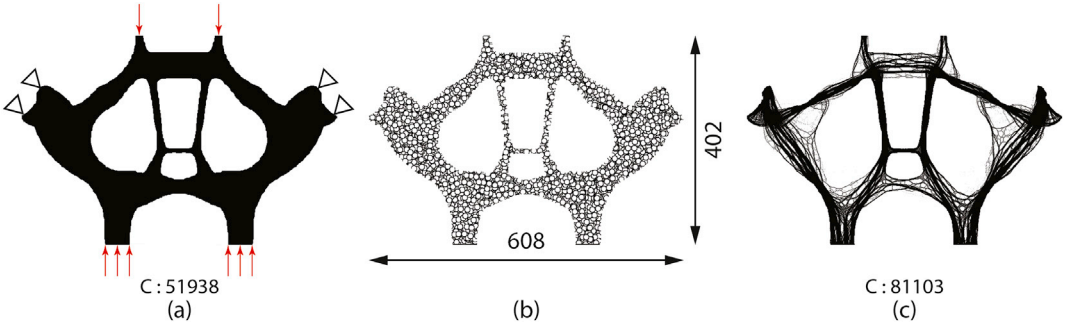

Fig. 18. Human midface implant problem. (a) Design domain and boundary conditions, (b) Initial density distribution used in the analysis ($P = 46,187$), (c) Topology optimization result with perimeter control constraint ($P_{min} = 30,000$). Volume fraction constraint of 20% is used. 80% volume decrease led to a 56% increase in the compliance value.

engineering problem that requires geometric complexity to cope with uncertainties in the design domain and to promote reliable structures with high porosity. For example, issues with stress shielding and inadequate mass transfer in medical implant industry could be tackled with the technique described in this work.

6. Conclusions

We present a topology optimization approach with perimeter control to obtain the complex bone internal structure. In order to obtain the natural design of bones, a regulation on solution space is necessary. A constraint-based restriction approach that gives the user control on the perimeter measure in the solution is presented. The approach can also be used to design complex porous structures. A lower bound in the perimeter of a structure is introduced in the topology optimization formulation to control the fine members in the final design. Numerical issues such as gray regions, checkerboards, or density islands are common with uniform initial density distribution when very low or very high perimeter values are chosen as the target. These numerical issues can be alleviated by introducing controlled randomness in the initial design using the perimeter constraint. The convergence can be improved without any undesired numerical artifacts or instabilities. Natural looking configurations with various curvatures can be obtained, and this makes the presented approach suitable for mimicking geometrically complex natural designs. Results from numerical examples using three different bone regions (femur, calcaneus, and mid-face) show agreements with X-ray scans. This methodology is expected to be useful in addressing mechanical property mismatch issue between the implant and its neighboring bones. The proposed approach can also be used in reverse-engineering the natural design principles by investigating the dominating loads to generate such design. The study shown in this work can be considered as a *proof of concept* as it only deals with simplified 2D problems. Authors are currently extending this idea to so it can address problems involving 3D space. Efficient solver with parallelization may be necessary in order to handle larger system matrices.

Acknowledgement

This research was partially funded by the National Science Foundation grants No. 1521801 and No. 1559594 (formerly No.1335160) and by Veteran Affairs grant No. 5I01 BX000418-06. We are grateful for the endowment provided by the Raymond Allen Johns Chair at the Georgia Institute of Technology. Authors also acknowledge Professor Krister Svanberg for providing the MMA code. We thank Mr. Erol Unal for useful suggestions in the manuscript. The opinions, findings, and conclusion stated herein are those of the authors and do not necessarily reflect those of sponsors.

References

[1] T. M. Ryan, C. N. Shaw, Unique suites of trabecular bone features characterize locomotor behavior in human and non-human anthropoid primates, PLoS One 7(7).
[2] H. Chirchir, H. Dean, K. Carlson, C. Ruff, Revisiting the evolution of low trabecular bone density in modern humans, FASEB J. 31 (2017) 251–253.
[3] H. Weinans, R. Huiskes, H. Grootenboer, The behavior of adaptive bone-remodeling simulation models, J. Biomech. 25 (12) (1992) 1425–1441.
[4] I. G. Jang, I. Y. Kim, B. M. Kwak, Analogy of strain energy density based bone-remodeling algorithm and structural topology optimization, J. Biomech. Eng. Trans. ASME 131(1).
[5] P. Christen, K. Ito, R. Ellouz, S. Boutroy, E. Sornay-Rendu, R. D. Chapurlat, B. Van Rietbergen, Bone remodelling in humans is load-driven but not lazy, Nat. Commun. 5.
[6] L.E. Lanyon, C. Rubin, Static vs dynamic loads as an influence on bone remodelling, J. Biomech. 17 (12) (1984) 897–905.
[7] S. Cowin, D. Hegedus, Bone remodeling i: theory of adaptive elasticity, J. Elasticity 6 (3) (1976) 313–326.
[8] D.R. Carter, W.C. Hayes, The compressive behavior of bone as a two-phase porous structure, JBJS 59 (7) (1977) 954–962.
[9] D. Fyhrie, D. Carter, A unifying principle relating stress to trabecular bone morphology, J. Orthop. Res. 4 (3) (1986) 304–317.
[10] R. Huiskes, H. Weinans, H. Grootenboer, M. Dalstra, B. Fudala, T. Slooff, Adaptive bone-remodeling theory applied to prosthetic-design analysis, J. Biomech. 20 (11–12) (1987) 1135–1150.
[11] H. Weinans, R. Huiskes, H. Grootenboer, The mechanical effects of fibrous tissue interposition at the cement-bone interface in tha, Trans. Orthop. Res. Soc. 13 (1988) 502.
[12] G. Beaupré, T. Orr, D. Carter, An approach for time-dependent bone modeling and remodeling theoretical development, J. Orthop. Res. 8 (5) (1990) 651–661.
[13] C. Oldani, A. Dominguez, Titanium as a biomaterial for implants, in: Recent Advances in Arthroplasty, InTech, 2012.
[14] K. Haase, G. Rouhi, Prediction of stress shielding around an orthopedic screw: using stress and strain energy density as mechanical stimuli, Comput. Biol. Med. 43 (11) (2013) 1748–1757.
[15] I. Levadnyi, J. Awrejcewicz, M.F. Goethel, A. Loskutov, Influence of the fixation region of a press–fit hip endoprosthesis on the stress–strain state of the bone–implant system, Comput. Biol. Med. 84 (2017) 195–204.
[16] S.-F. Huang, L.-J. Lo, C.-L. Lin, Biomechanical optimization of a custom-made positioning and fixing bone plate for le fort i osteotomy by finite element analysis, Comput. Biol. Med. 68 (2016) 49–56.
[17] P.-I. Tsai, C.-C. Hsu, S.-Y. Chen, T.-H. Wu, C.-C. Huang, Biomechanical investigation into the structural design of porous additive manufactured cages using numerical and experimental approaches, Comput. Biol. Med. 76 (2016) 14–23.
[18] M. Moesen, Modeling of the Geometry and Mechanical Behavior of Bone Scaffolds, Ph.D. thesis, Katholieke Universiteit Leuven, 2009.
[19] M.P. Bendsoe, O. Sigmund, Topology Optimization: Theory, Methods, and Applications, second ed., Springer, 2004.
[20] M.P. Bendsøe, O. Sigmund, Topology optimization by distribution of isotropic material, in: Topology Optimization, Springer, 2004, pp. 1–69.
[21] O. Sigmund, S. Torquato, Design of smart composite materials using topology optimization, Smart Mater. Struct. 8 (3) (1999) 365.
[22] H.A. Eschenauer, N. Olhoff, Topology optimization of continuum structures: a review, Appl. Mech. Rev. 54 (4) (2001) 331–390.
[23] L. Krog, A. Tucker, M. Kemp, B. R, Topology optimization of aircraft wing box ribs, in: The Altair Technology Conference 2004, 2004.
[24] M. Cavazzuti, A. Baldini, E. Bertocchi, D. Costi, E. Torricelli, P. Moruzzi, High performance automotive chassis design: a topology optimization based approach, Struct. Multidiscip. Optim. 44 (1) (2011) 45–56.
[25] X. Huang, Y.M. Xie, G. Lu, Topology optimization of energy-absorbing structures, Int. J. Crashworthiness 12 (6) (2007) 663–675.
[26] E. Norberg, S. Lovgren, Topology Optimization of Vehicle Body Structure for Improved Ride & Handling, Thesis, 2011.
[27] J.M. Rossi, S. Wendling-Mansuy, A topology optimization based model of bone adaptation, Comput. Meth. Biomech. Biomed. Eng. 10 (6) (2007) 419–427.
[28] Z. Xinghua, G. He, G. Bingzhao, The application of topology optimization on the quantitative description of the external shape of bone structure, J. Biomech. 38 (8) (2005) 1612–1620.
[29] I.G. Jang, I.Y. Kim, Computational simulation for trabecular adaptation in human proximal femur using design space optimization, in: 12th AIAA/ISSMO Multidisciplinary Analysis and Optimization Conference, 2008.
[30] I.G. Jang, I.Y. Kim, Computational study of wolff's law with trabecular architecture in the human proximal femur using topology optimization, J. Biomech. 41 (11) (2008) 2353–2361.
[31] I.G. Jang, I.Y. Kim, Computational study on the effect of loading alteration caused by disc degeneration on the trabecular architecture in human lumbar spine, J. Biomech. 43 (3) (2010) 492–499.
[32] M. Bagge, A model of bone adaptation as an optimization process, J. Biomech. 33 (11) (2000) 1349–1357.
[33] R.B. Haber, C.S. Jog, M.P. Bendsoe, A new approach to variable-topology shape design using a constraint on perimeter, Struct. Optim. 11 (1) (1996) 1–12.
[34] M.P. Bendsoe, N. Kikuchi, Generating optimal topologies in structural design using a homogenization method, Comput. Meth. Appl. Mech. Eng. 71 (2) (1988) 197–224.
[35] M.P. Bendsoe, O. Sigmund, Material interpolation schemes in topology optimization, Arch. Appl. Mech. 69 (9–10) (1999) 635–654.
[36] E. Andreassen, A. Clausen, M. Schevenels, B.S. Lazarov, O. Sigmund, Efficient topology optimization in matlab using 88 lines of code, Struct. Multidiscip. Optim. 43 (1) (2011) 1–16.
[37] K. Svanberg, The method of moving asymptotes - a new method for structural optimization, Int. J. Numer. Meth. Eng. 24 (2) (1987) 359–373.
[38] G.I.N. Rozvany, A critical review of established methods of structural topology optimization, Struct. Multidiscip. Optim. 37 (3) (2009) 217–237.
[39] O. Sigmund, On the usefulness of non-gradient approaches in topology optimization, Struct. Multidiscip. Optim. 43 (5) (2011) 589–596.
[40] A. Diaz, O. Sigmund, Checkerboard patterns in layout optimization, Struct. Optim. 10 (1) (1995) 40–45.
[41] O. Sigmund, J. Petersson, Numerical instabilities in topology optimization: a survey on procedures dealing with checkerboards, mesh-dependencies and local minima, Struct. Optim. 16 (1) (1998) 68–75.
[42] G.S. Beaupre, T.E. Orr, D.R. Carter, An approach for time-dependent bone modeling and remodeling - application - a preliminary remodeling simulation, J. Orthop. Res. 8 (5) (1990) 662–670.
[43] K. Tsubota, T. Adachi, Y. Tomita, Functional adaptation of cancellous bone in human proximal femur predicted by trabecular surface remodeling simulation toward uniform stress state, J. Biomech. 35 (12) (2002) 1541–1551.
[44] H.A. Kim, P.J. Clement, J.L. Cunningham, Investigation of cancellous bone architecture using structural optimisation, J. Biomech. 41 (3) (2008) 629–635.

[45] A. Sutradhar, G.H. Paulino, M.J. Miller, T.H. Nguyen, Topological optimization for designing patient-specific large craniofacial segmental bone replacements, Proc. Natl. Acad. Sci. U. S. A 107 (30) (2010) 13222–13227.
[46] A. Sutradhar, J. Park, D. Carrau, T.H. Nguyen, M.J. Miller, G.H. Paulino, Designing patient-specific 3d printed craniofacial implants using a novel topology optimization method, Med. Biol. Eng. Comput. 54 (7) (2016) 1123–1135.
[47] J. Park, Topology Optimization to Design Bone Replacement Shapes in Craniofacial Reconstructive Surgery: Design, Simulation and Experimental Validation, Master's thesis, The Ohio State University, 2013.
[48] A. Sutradhar, J. Park, D. Carrau, M.J. Miller, Experimental validation of 3d printed patient-specific implants using digital image correlation and finite element analysis, Comput. Biol. Med. 52 (2014) 8–17.
[49] J. Garcia, M. Martinez, M. Doblaré, An anisotropic internal-external bone adaptation model based on a combination of cao and continuum damage mechanics technologies, Comput. Meth. Biomech. Biomed. Eng. 4 (4) (2001) 355–377.
[50] M. Doblaré, J. Garcıa, Application of an anisotropic bone-remodelling model based on a damage-repair theory to the analysis of the proximal femur before and after total hip replacement, J. Biomech. 34 (9) (2001) 1157–1170.
[51] T.P. Harrigan, J.J. Hamilton, Bone remodeling and structural optimization, J. Biomech. 27 (3) (1994) 323–328.
[52] S.J. Hollister, J. Brennan, N. Kikuchi, A homogenization sampling procedure for calculating trabecular bone effective stiffness and tissue level stress, J. Biomech. 27 (4) (1994) 433–444.
[53] C.R. Jacobs, J.C. Simo, G.S. Beaupre, D.R. Carter, Adaptive bone remodeling incorporating simultaneous density and anisotropy considerations, J. Biomech. 30 (6) (1997) 603–613.
[54] A. Tovar, Bone Remodeling as a Hybrid Cellular Automaton Optimization Process, Ph.D. thesis, 2004.
[55] R. Huiskes, If bone is the answer, then what is the question? J. Anat. 197 (2) (2000) 145–156.